Dalton Transactions

Accepted Manuscript

ROYAL SOCIETY OF CHEMISTRY

www.rsc.org/dalton

Graphical Abstract

Synthesis, structures and magnetic properties in 3d-electron-rich isostructural complexes based on chains with sole syn-anti carboxylate bridges

Feng Su[a], Liping Lu*[a], Sisi Feng[a], Miaoli Zhu*[a,b] and Zengqiang Gao[c], Yuhui Dong[c]

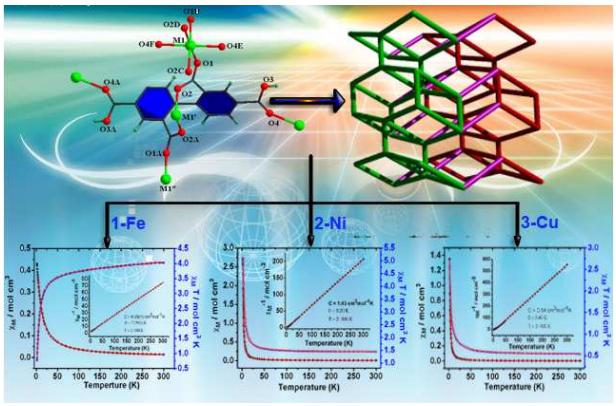

A series of isostructures based on 2,2',4,4'-biphenyltetracarboxylic acid have been synthesized via solvothermal reaction, whereas magnetic studies reveal the polymers with isostructural features and a uniform chain model with sole *syn−anti* carboxylate bridges show different magnetic behaviors.

Journal Name

RSCPublishing

ARTICLE

Synthesis, structures and magnetic properties in 3d-electron-rich isostructural complexes based on chains with sole syn-anti carboxylate bridges

Cite this: DOI: 10.1039/x0xx00000x

Received 00th January 2012,
Accepted 00th January 2012

DOI: 10.1039/x0xx00000x

www.rsc.org/

Feng Su[a], Liping Lu*[a], Sisi Feng[a], Miaoli Zhu*[a,b], Zengqiang Gao[c] and Yuhui Dong[c]

To evaluate magnetic properties of isostructural compounds, a series of 3D carboxylate coordination polymers $[M(H_2bpta)]_n$, (H_4bpta = 2,2',4,4'-biphenyltetracarboxylic acid, M = Fe(II) **(1)**, Ni(II) **(2)**, Cu(II) **(3)** and Zn(II) **(4)**), have been synthesized in H_2O/CH_3CN or H_2O solvents, respectively. Structurally, complexes **1**–**4** have isostructural features with (5,5)-connected 3D framework, wherein the M(II) centre takes octahedral coordination environment consisting of six oxygen atoms from carboxylates of ligands. The M(II) sites are linked by *syn-anti* carboxylates to form chains with a M···M separation of 4.880(2) (M = Fe), 4.784(2) (M = Ni), 4.541(2) (M = Cu), and 4.607(2) Å (M = Zn), respectively. The shortest M···M distances between inter-chains locate 9.122(4), 9.077(3), 9.361(3) and 8.767(2) Å, respectively. Magnetically, the isostructural polymers show different magnetic behaviors due to different spins of central ions. Theoretical analysis indicates that couplings between magnetic ions obey uniform chain models. The magnetic susceptibility of **1** and **2** are perfectly fitted by the modified Fisher model to yield an effective intra-chain exchange coupling constant of –0.81(1) and 3.67(2) cm^{-1}, respectively. For **3**, a Heisenberg ferromagnetic S = 1/2 chain included the intrachain magnetic exchange interaction (J = 9.28(1) cm^{-1}, and zj' = –0.068(3) cm^{-1}) reports weak ferromagnetic interactions in intrachains and weak antiferromagnetic interactions between interchains. The phenomena of **1**–**3** accord with the common view that the exchange interaction between two magnetic M(II) ions bridged by the *syn-anti* carboxylate bridge is dominantly weak ferro- or antiferromagnetic interactions. In addition, the M–O–C–O–M spin exchange interactions $|J|$ of $M_2(CO_2)_2$ (M = Mn($3d^5$)[20], Fe($3d^6$), Co($3d^7$)[20], Ni($3d^8$), Cu($3d^9$)) decrease strengthes with $Cu_2(CO_2)_2$ > $Ni_2(CO_2)_2$ > $Co_2(CO_2)_2$ > $Fe_2(CO_2)_2$ > $Mn_2(CO_2)_2$, consistent with the orbits order.

Introduction

Coordination polymers (CPs) have gathered considerable attention for decades not only because of their intriguing diversity of architectures and topologies,[1] but also due to the potential applications in selective guest inclusion, chirality, catalysis, nonlinear optics, luminescent, magnetism, and possible applications in other areas.[2] Rational selection of metal centers and organic ligands plays a significant role in the assembly of CPs with exhibiting targeted chemical and physical properties.[3] Usually, the flexible diamagnetic ligands are used to link magnetic d or f metal ions into extend networks, facilitating magnetic exchange in one-, two-, and three-dimensions.[4] In the CPs, there are self-assemblies of isostructural or isotopological[5] compounds, which provide variations of magnetic anisotropy and spin quantum numbers that affect the magnetic behavior of such isostructural systems, such as $[Ni_2(1,4\text{-bib})_2(m,p\text{-bpta})(H_2O)_2]$ (M = Co(II), and Ni(II); *m,p*-bpta = 3,3',4,4'-biphenyltetracarboxylic acid, and 1,4-bib = 1,4-bis(imidazol-1-yl)benzene)[6a], $[M(l\text{-tartrate})]_n$ (M = Mn(II), Co(II), Fe(II), and Ni(II); l-tartrate = (2R, 3R)-(+)-tartrate)[6b], $[M(HL)(hfac)]_n$ (M = Mn(II), Ni(II), and Cu(II); hfac = hexafluoroacetylacetonate anion)[6c], $M(HCOO)_2(4,4'\text{-bpy})\cdot nH_2O$ (M = Co(II), and Ni(II))[6d], and $[M(L)(N_3)]_n\cdot 3nH_2O$ (M = Mn(II), Co(II), and Ni(II); L^- = 1-(4-carboxylatobenzyl-pyridinium-4-carboxylate)[6e]. The magnetic interactions

[a]Institute of Molecular Science, Key Laboratory of Chemical Biology and Molecular Engineering of the Education Ministry, Shanxi University, Taiyuan, Shanxi 030006, P. R. China.
[b]State Key Laboratory of Coordination Chemistry, Nanjing University, Nanjing 210093, P. R. China.
[c]*Beijing Synchrotron Radiation Facility, Institute of High Energy Physics, Chinese Academy of Sciences, Beijing, 100049, P. R. China.*
Institute of Molecular Science, Shanxi University, 92 Wucheng Road, Taiyuan, Shanxi 030006, P. R.China. Tel: ++86-351-7017974; Fax: ++86-351-7011022; E-mail: luliping@sxu.edu.cn miaoli@sxu.edu.cn

between transition metal centers usually is mediated through two types of spin exchange paths, namely, M–L–M super-exchange and/or M–L···L–M super-superexchange paths. [7] As for the former, M–L–M superexchange is important in magnetic orbits of metal ions, in which the nd-orbits of metal ions are combined out-of-phase with the np-orbits of ligands. The latter can be much weaker than M–L–M superexchanges in leading to magnetic interactions. The orbital interaction plays a significant role in the spin Hamiltonian for a given magnetic system. Indeed, a pretty large number of coordination polymers with magnetic properties have been reported, due to the use of constitutive open-shell transition metal ions within the framework of the structure. The strength of a given M–L···L–M spin exchange may be apparently determined by the shortness of the M···M distance.[8]

With this in mind, the aromatic acids seem to be an excellent choice toward building blocks of higher-nuclearity structures[4a, 9] and an efficient magnetic exchange pathway in paramagnetic dinuclear or polynuclear transition-metal complexes.[10] Over the last decades, a huge number of metal complexes with diverse bridging modes such as μ_2-η^2 and μ_2-η^1:η^1 (*syn-syn*/*syn-anti*/*anti-anti*) modes of COO^- and various types of structures from chains, layers, and networks have been reported,[5b, 7c, 8d, 11] which exhibit different structures and interesting magnetic properties. As a result, the polycarboxylic acid ligands contain several hard O,O-chelating sites, which can bond to a great number of metal ions to form metal ion clusters.[12] In addition, the carboxylic groups can assume many kinds of bridging or multidentate chelating modes to construct CPs. One of them, 2,2',4,4'-biphenyl-tetracarboxylic acid (H_4bpta) with C_2 symmetry has recently attracted attention owing to its above advantageous, which accessibility connects metal ions to form indefinite ribbon chain structure due to the ortho-carboxyl chelation. Thus, the magnetic system described by a Heisenberg spin Hamiltonian undergoes a 1D long-range magnetic order. To our knowledge, only a few Cu(II) complexes with sole *syn-anti* carboxylate-bridged have been reported so far,[13] which usually exhibit ferromagnetic exchange coupling and in a few instances exhibit antiferromagnetic coupling, whereas, magneto-structural studies on similar Fe(II)/Ni(II) complexes are scarce. As compared to the very similar compound $[Fe(pyoa)_2]_n$ (pyoa = 2-(pyridin-3-yloxy)acetate)[14], the Jahn-Teller effect in an octahedral geometry plays a vital role to magnetic behavior.

Herein, to analyze magnetic properties of isostructural complexes as well as sole *syn-anti* carboxylate bridging manner leading to magnetic effects, we succeeded in obtaining four new three-dimensional polynuclear complexes $[Fe(H_2bpta)]_n$ **(1)**, $[Ni(H_2bpta)]_n$ **(2)**, $Cu(H_2bpta)]_n$ **(3)**, and $[Zn(H_2bpta)]_n$ **(4)** with one-dimensional uniform chain, in which the carboxylate shows *syn-anti* basal-basal bridging mode. The variable-temperature magnetic measurement reveals that the complex **1** shows a weak antiferromagnetic interaction and both **2** and **3** exhibit ferromagnetic exchange interaction through the *syn-anti* bridging mode.

Experimental

General Methods and Materials

H_4bpta = 2,2',4,4'-biphenyltetracarboxylic acid was received from Jinan Camolai Trading Company, China. Other reagents and solvents were of standard commercial grade and directly used without further purification. IR spectra were obtained on a BRUKEP TENSOR27 spectrometer with KBr disks. Elemental analysis was performed by CHNO-Rapid instrument. Powder X-ray diffraction (XRD) data were collected on a Bruker D8 Advance X-ray diffractometer with Cu Kα radiation (λ = 1.5418 Å). Thermogravimetric (TG) studies were carried out on a Dupont thermal analyzer with temperature range 25−825 °C under air flow with a heating rate of 20 °C min^{-1}. Magnetic susceptibility measurements data were obtained with SQUID magnetometer (Quantum MPMS) in the temperature range 2.0−300 K by using an applied field of 1000 *Oe*.

Synthesis of Complexes

$[Fe(H_2bpta)]_n$ (1). A mixture of H_4bpta (33.0 mg, 0.1 mmol), $Fe_2(SO_4)_3$ (80.0 mg, 0.2 mmol), $H_2C_2O_4$(18.0 mg, 0.2 mmol) and 6 mL of H_2O/CH_3CN (2:1, v/v) was placed in a 13 mL Teflon-lined stainless steel autoclave. The mixture was heated under autogenous pressure at 160 °C for 72 h and then cooled to room temperature. Yellow block-shaped crystals of **1** were collected by filtration, washed with H_2O, and dried in air. Yield ~57%. Anal. Calcd for $C_{16}H_8O_8Fe$: C 50.03, H 2.10. Found: C 49.98, H 2.12. IR (cm^{-1}, s for strong, m medium, w weak): 3519m, 3166m, 2642m, 1699s, 1611m, 1561w, 1419s, 1281m, 1215m, 1102w, 1005w, 775m, 677w, 651w.

$[Ni(H_2bpta)]_n$ (2). A mixture of H_4bpta (33.0 mg, 0.1 mmol), $NiCl_2·6H_2O$ (47.4 mg, 0.2 mmol) and 8 mL of water was placed in a 13 mL Teflon-lined stainless steel autoclave. The mixture was heated under autogenous pressure at 150 °C for 72 h and then cooled to room temperature. Green block-shaped crystals of **2** were collected by filtration, washed with H_2O followed by acetone, and dried in air. Yield ~64%. Anal. Calcd for $C_{16}H_8O_8Ni$: C 49.67, H 2.08. Found: C 49.69, H 2.03. IR (cm^{-1}): 3440w, 3080w, 2362w, 1922w, 1635s, 1551m, 1474m, 1417s, 1370s, 1293m, 1243s, 1169w,1050w, 851w, 811w, 698m, 527m.

$[Cu(H_2bpta)]_n$ (3). Following the procedure adopted from $NiCl_2·6H_2O$ to $CuCl_2·2H_2O$ with everything else kept the same as in **2**, azury block-shaped crystals of **3** were formed. Yield ~54%. Anal. Calcd for $C_{16}H_8O_8Cu$: C 49.05, H 2.06. Found: C 49.01, H 2.10. IR (cm^{-1}): 3435w, 3072w, 2886m, 1684s, 1608m, 1569m, 1540s, 1476m, 1428s, 1396m, 1371s, 1270m, 1231s, 1123m, 932w, 729w, 692m, 651m, 515m.

$[Zn(H_2bpta)]_n$ (4). Following the procedure adopted from $NiCl_2·6H_2O$ to $ZnCl_2·6H_2O$ with everything else kept the same as in **2**, pale yellow block-shaped crystals of **4** were formed. Yield ~61%. Anal. Calcd for $C_{16}H_8O_8Zn$: C 48.82, H 2.05. Found: C 48.87, H 2.04. IR (cm^{-1}): 3436w, 3080w, 2404m, 1898m, 1647s, 1560s, 1418s, 1371s, 1294m, 1244s, 1167w, 1004m, 851m, 804m, 771m, 694m, 524m.

X-ray Crystallography

The data of the complex **1** was collected on a Bruker Smart Apex II diffractometer equipped with 1 K CCD instrument by using a graphite monochromator utilizing Mo-Ka radiation (λ = 0.71073 Å) at RT. Cell parameters were determined using SMART software.[15] Data reduction and correction was performed using SAINTPlus.[16] Absorption correction was made *via* SADABS.[17]

Single-crystal X-ray diffraction data for complexes **2**−**4** were collected in Beijing Synchrotron Radiation Facility (BSRF) beamline 3W1A which mounted with a MARCCD-165 detector (λ = 0.72000 Å) with storage ring working at 2.5 GeV. A single crystal of **2**−**4** of size approximately 0.1 × 0.1 × 0.1 mm^3 were selected for the data collection. In the process, the crystals were protected by liquid nitrogen at 173(2) K. Data were collected by the program MARCCD and processed using HKL 2000.[18]

All the structures were solved by direct methods employed in the programs SHELXS-97[19] and refined by full-matrix least-squares methods against F^2 with SHELXL-97.[19] All the non-H atoms were refined anisotropically. Hydrogen atoms attached to C and O atoms were placed geometrically and refined using a riding model approximation, with C−H = 0.93−0.96 and O−H = 0.82 Å. A summary of the crystallographic data and data collection and refinement parameters for all compounds are provided in Table 1. Crystallographic data in CIF format were deposited with the Cambridge Crystallographic Data Center as CCDC 1032513−1032516 for **1**−**4**, respectively.

Table 1 Crystal data and structure refinement parameters for compounds **1**−**4**

Compound	**1**	**2**	**3**	**4**
CCDC	1032513	1032514	1032515	1032516
Formula	$C_{16}H_8O_8Fe$	$C_{16}H_8O_8Ni$	$C_{16}H_8O_8Cu$	$C_{16}H_8O_8Zn$
Fw	384.07	386.93	391.76	393.59
Temp (K)	298(2)	173(2)	173(2)	173(2)
Wavelength(Å)	0.71073	0.72000	0.72000	0.72000
Crystal system	Orthorhombic	Orthorhombic	Orthorhombic	Orthorhombic
Space group	*Pbcn*	*Pbcn*	*Pbcn*	*Pbcn*
a (Å)	15.772(2)	15.680(3)	16.160(3)	15.147(3)
b (Å)	9.1710(14)	9.1490(18)	9.4550(19)	8.8340(18)
c (Å)	9.6050(14)	9.4150(19)	8.9840(18)	9.0620(18)
Vol ($Å^3$)	1389.3(4)	1350.6(5)	1372.7(5)	1212.6(4)
Z	4	4	4	4
D_c (g/cm^3)	1.836	1.903	1.896	2.156
μ(mm^{-1})	1.134	1.486	1.640	2.081
F(000)	2288	2192	960	462
R_1 [$I>2\sigma(I)$], wR_2 (all data)	0.0384, 0.0983	0.0297, 0.0763	0.0362, 0.1014	0.0678, 0.1689
GOF on F_2	1.097	1.278	1.104	1.116
$\rho_{max, min}$, e ($eÅ^{-3}$)	0.281/−0.338	0.540/−0.726	0.572/−1.211	2.293/−2.039

$$R_1 = \sum \frac{||F_o| - |F_c||}{|F_o|}, \quad wR_2 = \sqrt{\frac{\sum w(F_o^2 - F_c^2)^2}{\sum w(F_o^2)^2}}$$

Journal Name RSCPublishing

ARTICLE

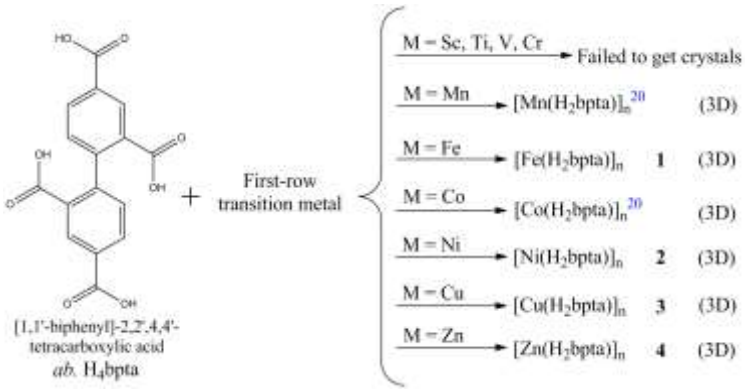

Scheme 1 Diagram of synthesis and known relative complexes

Results and discussion

Sythesis and Characterization of 1–4

In the initial recipes, we were going to employ the H_4bpta ligand to coordinate to first transition metal ions. The self-assembly process of **1**–**4** with 3d-electron-rich metal ions was achieved as set out in Scheme 1, in which we merged search results from previous literature[20]. A rational approach to the design and synthesis of complexes is critical. In the process of the synthesis, the complex **1** is different from the others due to the redox reaction for Fe(II)/Fe(III) to avoid impurity of Fe(III). Hence, the complex **1** was synthesised by Fe^{2+} added $H_2C_2O_4$ in the H_2O/CH_3CN solvent. **2**–**4** were successfully achieved by a mixture of MCl_2 (M =Ni, Cu, and Zn), and H_4bpta in aqueous solution. Unfortunately, we failed to receive suitable crystal products of other metal ions with $3d^{1\text{-}4}$ electronic configuration although great efforts made.

IR spectra of the complexes were examined and given in Fig. S1 (Supporting Information), in which the absorption bands show the characteristic stretching vibrations of COO^-, O–H and aromatic C–H groups. The fact that the COO^- is coordinated with its asymmetric $\nu_{(OCO)assym}$ (1650, 1637, 1686, 1646 and 1643 cm^{-1}, respectively) and symmetric $\nu_{(OCO)sym}$ (1413, 1418, 1431, 1418, and 1401 cm^{-1}, respectively) stretching appearing at 1686–1637cm^{-1} and 1431–1401 cm^{-1} for the complexes **1**–**4**, respectively. The $\Delta\nu(\nu_{(OCO)assym} - \nu_{(OCO)sym})$ is 219–255 cm^{-1}, showing the presence of bidentate linkage of carboxylate in the anion ligand. Compared with free ligand, the broad band at 3443 cm^{-1} indicates the stretching vibration of ortho/para-position carboxyl groups O–H , which consists with the partial deprotonation of the carboxylic groups of the H_4bptc ligand in the complexes **1**–**4**. The band at about 3084 cm^{-1} is attributed to the stretching vibration of the aromatic C–H groups. These various frequencies may be related to the bridging mode of the carboxylate functions of H_2bpta^{2-} in these complexes.

TG/DSC analysis results (Fig. S2, Supporting Information) indicate that the complexes **1**–**4** are stable until about 424, 446, 365, and 407 °C, respectively, which corresponds to the endothermic peak at 468, 487, 415, and 434 °C on the DSC curves for **1**–**4**, respectively.

Powder X-ray diffraction (XRD) patterns of **1**–**4** were determined at room temperature, which match well with those simulated from their X-ray single crystal diffracting data, and the well purity of the complexes **1**–**4** (Fig. S3, Supporting Information) can be confirmed.

Description of the Crystal Structures $[M(H_2bpta)]_n$

The structures of the complexes **1**–**4** are isostructural, and thus, only the structure of representative complex **1** will be described in detail below. Complex **1** crystallizes in the orthorhombic space group *Pbcn* with the Fe(II) ions sitting on a 2-fold axis, which encompasses a half Fe(II) ion, and a half H_2bpta^{2-} anions in the asymmetric unit. In **1**, the Fe(II) ion is surrounded by six oxygen atoms from five H_2bpta^{2-} ligands to present an octahedron geometry. Wherein Fe(II) ions bridged the ortho-position carboxylate groups to form a slight "V-shaped" array of three Fe(II) ions (Fe1···Fe1′···Fe1″ = 159.5(1)°, Symmetry codes: ′ 1 − *x*, −*y*, −*z*; ″ *x*, *y*, 1 + *z*). (Fig. 1a) Each H_2bpta^{2-} ligand connects five metal atoms, with both two full deprotonated carboxylate groups (2,2'-COO^-) in the trans conformation adopting μ_2-η^1:η^1 modes to chelate one Fe(II) ion and both two nondeprotonated carboxylate moieties (4,4'-COOH) adopting monodentate fashions. Due to steric

hindrance, the dihedral angles of the phenyl ring planes along the pivotal 1,1'-bond (C7-C7A) of ligands is 73.6(4)°.

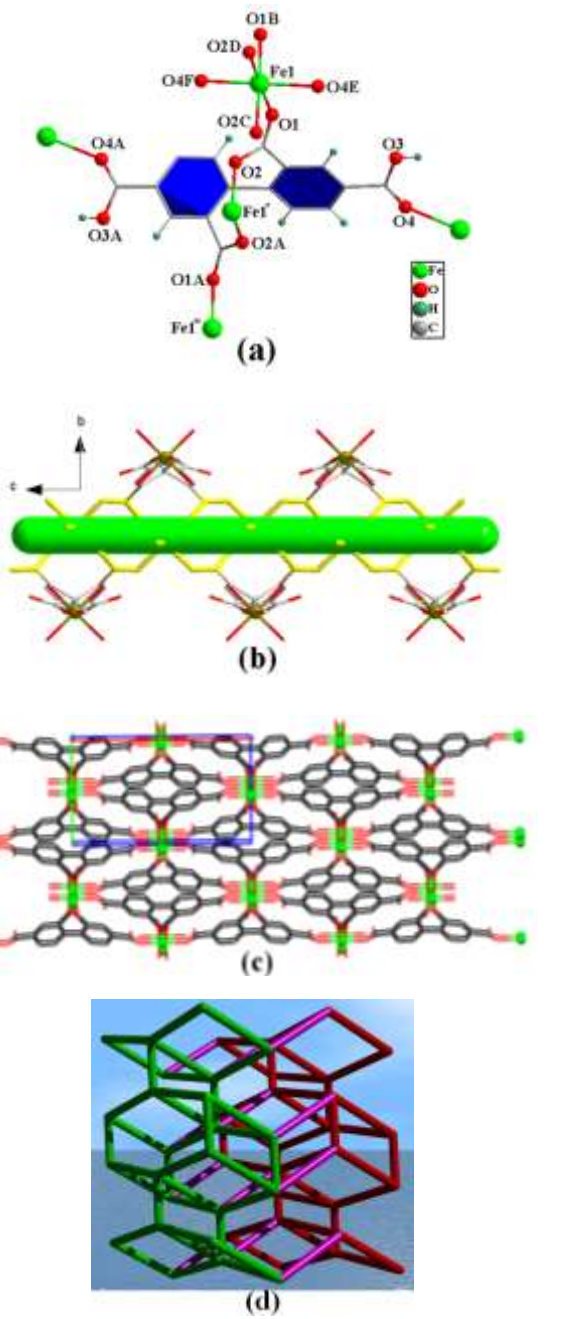

Figure 1 (a) Perspective view of the coordination of the Fe(II) ion for **1** with 'V-shaped' array of three Fe(II) ions. (Symmetry codes: A 1 − *x*, *y*, 1/2 − *z*; B 1 − *x*, *y*, −1/2 − *z*; C 1 − *x*, −*y*, −*z*; D *x*, −*y*, −1/2 + *z*; E 1/2 − *x*, 1/2 − *y*, −1/2 + *z*; F 1/2 + *x*, 1/2 − *y*, −*z*; ′ 1 − *x*, −*y*, −*z*; ″ *x*, *y*, 1 + *z*) (b) One-dimensional rob-like chain running along [001]. (c) Packing architecture hex-type rod-packing architecture (hydrogen atoms omitted for clarity). (d) A schematic representation of the (5,5)-connected topological network.

There is a common feature in these complexes, namely, all chelate carboxylates are sole *syn*−*anti* bridging mode. As shown in Fig. 1b, the Fe(II) ions are in-turn linked together by double *syn*−*anti* bridge carboxyl groups of H_2bpta^{2-}, resulting in the 1D rod-like arrangement of $[Fe_2(CO_2)_2]_n$ (separation of Fe···Fe, 4.880(2) Å) running along [001]. The Fe−O bond lengths are in the range of 2.100(2)−2.192(2) Å. The O−Fe−O angles are in the range of 84.07(8)−96.51(8)°. The $[Fe_2(CO_2)_2]_n$ rods are propagated by H_2bpta^{2-} ligands to form grid packing architecture (Fig. S4b, Supporting Information). It is worth noting that each $[Fe_2(CO_2)_2]_n$ rod connects six equivalent $[Fe_2(CO_2)_2]_n$ rods bridged by the carboxylate groups to generate the hexa-like rod-packing architecture via double organic spacers along the *c* axis. Ultimately, the structure represents a unique example of 3D networks with $[Fe_2(CO_2)_2]_n$ chains spaced by the H_2bpta^{2-} ligand. (Fig. 1c) In addition, such close hydrogen-bonding interactions between O3 atom and O2F atom (symmetry code: F *x* + 1/2, −*y* + 3/2, −*z* + 2) with a separation of 2.532(3) Å can efficiently strong intramolecular hydrogen bonds increase the stability of **1** (Table 2).

The coordination polymers of 2,2',4,4'-biphenyltetracarboxylate bound to 3d-electron-rich metal ions contain two types linear chains based on M−O−C−O−M or M−O−M[9a, 21] connections. The chains can be either separated or interlinked into 3D frameworks by multi-carboxylate ligands. In contrast, the bond lengths (M−O) for the complexes almost decrease with the increase of d-electronic number (Table 2) until full fill of d-electrons, agreeing with the radius variation of the metal ions, but the copper complex singularly occurred due to the Jahn-Teller effect. Meanwhile, two adjacent metal ions are linked by the double carboxyl bridges to form a $[M_2(CO_2)_2]$ ring with slight differences in the M···M distances (4.951(2) for Mn(II)[20], 4.880(2) (Fe(II)), 4.781(2) (Co(II))[20], 4.784(2) (Ni(II)), 4.541(2) (Cu(II)), & 4.607(2) Å (Zn(II)), respectively), (Table 2) which are all in agreement with reported values for the first transition metal multi-carboxyl complexes.[12d, 12e, 22] The shortest inter-chain M···M distances are 9.103(3), 9.122(4), 9.088(2), 9.077(3), 9.361(3) and 8.767(2) Å, respectively. Comparing with the different distances, the short intra-chain distances between the metal ions make the magnetic interaction more efficient and may lead to the 1D long-range order along the *c*-direction. (Fig. S4, Supporting Information) Due to the 2,2'-carboxylate chelation, the neighboring phenyl rings are tilted to form dihedral angles of 70.85(2), 73.59(4), 75.70(3), 74.72(4), 86.36(4), and 75.61(1)° for Mn to Zn, respectively.

Journal Name RSCPublishing

ARTICLE

Table 2 Comparing the bond distances (Å) and angles (°) around the metal centers in the isostructural polymers

	Mn(II)	Fe(II)	Co(II)	Ni(II)	Cu(II)	Zn(II)
M–O1	2.144(2)	2.100(2)	2.065(4)	2.053(3)	1.971(1)	1.977(1)
M–O2B	2.181(2)	2.126(2)	2.077(3)	2.060(4)	1.981(4)	2.011(1)
M–O4D	2.210(2)	2.192(2)	2.161(5)	2.114(4)	2.439(5)	2.093(1)
M…M	4.951(2)	4.880(2)	4.781(2)	4.784(2)	4.541(2)	4.607(2)
O1–M–O1A	94.00(1)	94.36(2)	92.27(1)	91.21(6)	88.58(3)	92.35(4)
O1A–M–O2B	86.78(2)	86.68(2)	87.86(3)	87.82(4)	89.07(5)	87.84(4)
O2B–M–O2C	92.47(1)	92.38(1)	92.21(1)	93.33(6)	93.76(7)	92.15(6)
O1–M–O4D	85.65(8)	84.07(8)	83.17(7)	82.64(5)	81.92(5)	83.45(4
O1A–M–O4D	95.03(8)	96.51(8)	97.62(7)	98.16(5)	99.90(5)	98.34(4)
O2B–M–O4D	93.36(8)	93.53(8)	93.75(7)	94.34(4)	93.27(4)	93.46(4)
O2C–M–O4D	85.95(8)	85.88(8)	85.46(7)	84.88(4)	85.00(4)	84.76(4)
∠Ph–Ph	70.85(2)	73.59(4)	75.70(3)	74.72(4)	86.36(4)	75.61(1)
H-bond(D…A)	2.521(2)	2.533(3)	2.497(2)	2.498(4)	2.619(0)	2.422(1)
Ref	20	This work	20	This work	This work	This work

Symmetry transformations used to generate equivalent atoms: A −x + 1, y, −z − 1/2; B x, −y, z − 1/2; C −x + 1, −y, −z; D −x + 1/2, −y + 1/2, z − 1/2

From topological point of view, the frameworks of complexes **1**–**4** can be simplified by the application of a (5,5)-connected topological approach (Fig. 1d). Adjacent two metal ions are defined one inorganic node with 5-connected, and the H_2bpta^{2-} ligand is also 5-connected. Therefore, the 3D framework resulting from the adequate connection of organic nodes can be represented as a ($4.6^4.8.4^3.6^6.8^6$) net.

Magnetic Properties

In order to insight the magnetic changes in the isostructural polymers, magnetic measurements were carried out on well-crushed crystalline samples of **1**–**3** except complex **4** with diamagnetism. As carboxylate bridging unsaturated d-electronic metal ions can propagate magnetic properties, the complexes **1**–**3** were subjected to variable-temperature magnetic susceptibility measurements in the 2.0–300 K range with an applied magnetic field of 1000 *Oe.* As noted previous magneto-structural studies for the complexes with bridging *syn-anti* carboxylate groups have evidenced the magnitudes of the exchange-coupling constants are small and the exchange is ferro- and antiferromagnetic interactions.[5a, 23]

[Fe(H$_2$bpta)]$_n$ (1). As shown in Fig. 2. At 300 K, the $\chi_M T$ value of complex **1** is 4.03(1) cm^3 mol^{-1} K, which is larger than the spin-only $\chi_M T$ of 3.00 cm^3 mol^{-1} K expected for one isolated high-spin Fe(II) ion (g = 2.0 and S = 2). It is indicated that Fe(II) ions have a high spin state and a higher value than is presumably due to the orbital contribution. Upon cooling, the values of $\chi_M T$ gradually decrease to reach 0.036(3) cm^3 K mol^{-1} at 2.0 K, which indicates the presence of an antiferromagnetic interaction in **1**. In the temperature range of 2.0 to 300 K, the magnetic susceptibility obeys the Curie–Weiss law, $\chi = C/(T - \theta)$ with a Curie constant, C = 4.09(1) cm^3 mol^{-1} K, and a Weiss temperature, θ = −7.59(1) K. (Fig. 2, inset).

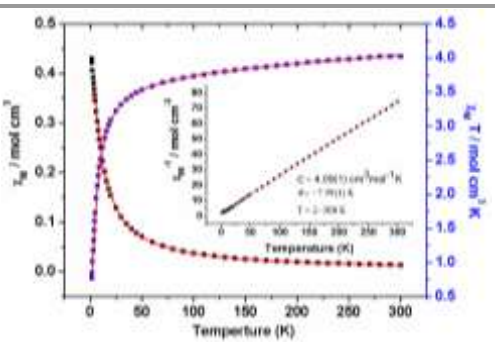

Figure 2 Temperature dependence of χ_M , $\chi_M T$, and 1/ χ_M collected in an applied field of 1000 K for complex **1**. The red solid line represents the best fittings.

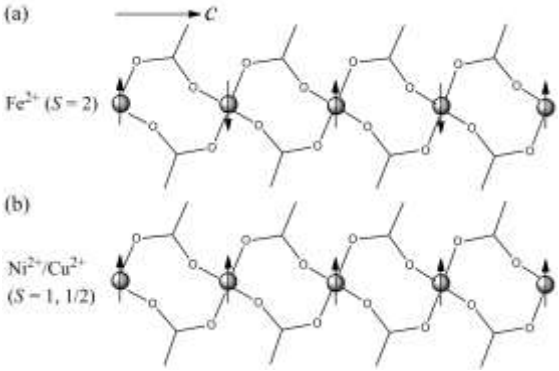

Scheme 2 The Magnetic exchange of intrachain via *syn-anti* bridging mode of the carboxylate ligand along the *c* axis of **1**–**3**.

As described above, the 3D structure encloses hexa-coordinated Fe(II) ions bound to H_2bpta^{2-} ligands. From magnetic point of view, the structure can be considered as a pseudo-one-dimensional linear spin-chain along the *c* axis with Fe(II) ions (distances of Fe…Fe, 4.880(2) Å, Scheme 2a and Fig. S4a, Supporting Information) linked by the bridges of 2,2'-dicarboxylates assumed that the coupling of the long bridging spaces (2,4 or 2',4'-dicarboxylic acids, distances of Fe…Fe, 9.122(4)) in adjacent chains in a given *bc* or *ac* layer of complex **1** (Figs. S4b and S4c, Supporting Information) being in a quasi negligible strength or molecular field approximation.

The *syn-anti* M−O−C−O−M could be dominating pathway to carry magnetic exchanges within the intrachain over the measured paramagnetic domain. The temperature dependence of the magnetic susceptibility of **1** is perfectly fitted by the modified Fisher model for a one-dimensional Heisenberg chain of $S = 2$ spins. The corresponding equation is given (eq 1)[24]:

$$\chi_{chain} = \frac{N_A g^2 \mu_B{}^2 S(S+1)}{3kT}\left[\frac{1+\mathrm{u}}{1-\mathrm{u}}\right] \qquad (1)$$

where *u* is the Langevin function:

$$\mathrm{u} = \coth\frac{JS(S+1)}{kT} - \frac{kT}{S(S+1)} \qquad (2)$$

J is the parameter of exchange interaction between two Fe(II) ions bridged by the carboxylate. An additional coupling parameter (*zj'*) represents the magnetic behaviour through H_2bptc^{2-} ligands interaction between the Fe–carboxylate linear spin-chain. The total magnetic susceptibility is:

$$\chi_M = \frac{\chi_{chain}}{1 - \frac{2zj' \times \chi_{chain}}{N_A g^2 \mu_B{}^2}} \qquad (3)$$

The best-fit well reproduces the experimental data over the whole temperature range with g = 2.25(2), J = −0.81(1) cm^{-1}, and zj' = −0.036(1) cm^{-1}, and the agreement factor defined by $R = \sum(\chi_M T_{exp} - x_M T_{cal})^2 / \sum(\chi_M T_{exp})^2$ is 8.9 × 10^{-4}. The g value is also in accord with expectation for Fe(II) complexes.[4e, 25] The negative θ and J values indicate the presence of weak antiferromagnetic interaction between adjacent Fe(II) ions.

According to the literature,[26] it can be deduced that the unpaired spin in e_g orbitals favor ferromagnetic interactions, whereas those in t_{2g} orbitals favor stronger antiferromagnetic interactions, with only one unpaired electron in a t_{2g} orbital being enough to dominate the overall superexchange. Therefore, Fe(II) complexes should show antiferromagnetic. Our result is in good agreement with these expectations.[8a] In addition, the low value of the exchange coupling constant, *J*, can be related to the nature of the bridge between neighboring Fe(II) ions. Comparing to recent studies of $[Fe(pyoa)_2]_n$ (pyoa = 2-(pyridin-3-yloxy)acetate)[14], we consider that weak ferromagnetic phenomenon might also exist in **1**, but it is opposite magnetic behavior. This can be related to the Jahn–Teller distortion. In $[Fe(pyoa)_2]_n$, a closer examination of the structural data strongly suggests that the origin of this sign reversal may be Jahn–Teller distortion, which is likely the main reason that the reorientation of the ordered spin state due to the movement of the domain wall,[27] so that an overall ferromagnetic behavior is observed. Whereas in complex **1** the Fe−O bond distances (see Table 2) are nearly close, thus not allowing for obvious Jahn–Teller distortion exits in the **1**. The value (J = −0.81(1) cm^{-1}) of the antiferromagnetic exchange interactions is somewhat less negative for the complex **1**, which is consistent with the *syn-anti* carboxylate bridge mediating weak magnetic coupling. Nevertheless, magneto-structural studies on hexa-coordinated Fe(II) complexes with the *syn-anti* carboxylate as a bridge are scarce, the authors can only compare their results with the one available Fe(II) compound with sole *syn-anti* coordination mode. **$[Ni(H_2bpta)]_n$ (2).** As shown in Fig. 3, the $\chi_M T$ value of 1.45 cm^3 K mol^{-1} at 300 K is a little larger than the spin-only value (1.00 cm^3 K mol^{-1}, g = 2.0 and S = 1) expected for isolated high-spin Ni(II) ions, assuming that the Ni(II) ion in the octahedral environment also has a small orbital contribution to the total magnetic moment.

The $\chi_M T$ value increases smoothly up to 1.81 cm^3 K mol^{-1} from room temperature to 20 K, and then the value rapidly increases to a maximum value of 5.11 cm^3 K mol^{-1} at 2.0 K. On the other hand, the magnetization value reaches 2.22 μB at 60 K*Oe* (Fig. S5, Supporting Information), which is slightly below the saturation value of 2.83 μ_B expected for a spin-only Ni(II) ion. It also corroborates the ferromagnetic coupling between Ni(II) ions. The data in the temperature range of

2.0−300 K obeys the Curie−Weiss law $\chi = C/(T - \theta)$ with C = 1.43 cm^3 K mol^{-1} and θ = 3.20 K. The deduced Curie constant per mole of Ni(II) agrees with the theoretical value of an S = 1 free ion (C = 1 cm^3 K mol^{-1} for isolated Ni(II)).

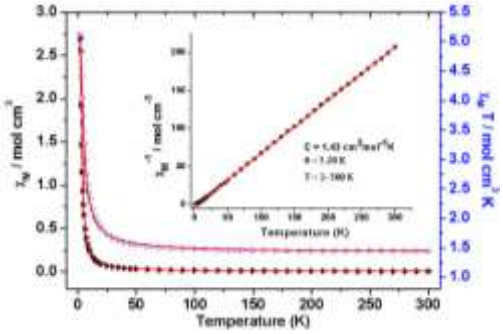

Figure 3 Temperature dependence of χ_M , $\chi_M T$, and 1/ χ_M collected in an applied field of 1000 K for complex **2**. The red solid line represents the best fittings.

Thus, the positive θ value is indicative of weak ferromagnetic interactions between adjacent Ni(II) ions in the network structure of **2**. Similarly, compared with the magnetic structure of **1** (Scheme 2b and Fig. S4, Supporting Information), **2** may be considered as uniform (J) coupling chains. The curve of magnetic susceptibility for **2** is perfectly defined via the Fisher infinite chain model (eq 1). The best-fit well reproduces the experimental data over the whole temperature range with g = 2.38(1), J = 3.67(2) cm^{-1}, zj' = −0.070(2) cm^{-1}, and $R = \sum(\chi_M T_{exp} - x_M T_{cal})^2 / \sum(\chi_M T_{exp})^2$ is 5.5 × 10^{-4}. The g value is also in accord with expectation for Ni(II) complexes.[5a] The θ > 0 and J > 0 values indicate the presence of a weak ferromagnetic exchange between Ni(II) centers in **2**. The Ni…Ni interactions between the spins S = 1 are transmitted through the *syn-anti* carboxylate bridges, and gives rise to a low ferromagnetic contribution. The *syn-anti* carboxylate bridging moiety has been observed in some Ni(II) complexes with ferromagnetic interactions reported elsewhere.[28] Whereas for Ni(II) system, the number of complexes with only *syn-anti* carboxylate conformations is much more less. Because the great tendency of Ni(II) ions to have, together with the carboxylate bridging ligands, other bridging ligands, like μ-oxo, μ-hydroxo, or μ-N_3.[29] Thus, the ferromagnetic coupling of the complex **2** with sole *syn-anti* carboxylate configuration seems to be in agreement with the results reported for copper(II) complexes.[30]

[Cu(H$_2$bpta)]$_n$ (3). The temperature dependence of $\chi_M T$ for complex **3** is shown in Fig. 4. At room temperature, the $\chi_M T$ value is about 0.54 cm^3 mol^{-1} K, which is slightly larger than the spin-only value (0.375 cm^3 mol^{-1} K) for S = 1/2. Upon cooling, the $\chi_M T$ value increases smoothly up to 0.26 cm^3 K mol^{-1} at 25 K, then increases very rapidly to reach a extreme value 2.50 cm^3 K mol^{-1} at 2.0 K, which indicates a characteristic feature of ferromagnetic coupling between Cu(II) ions. The corresponding experimental effective magnetization for Cu(II) is 1.14 μ_B (1.73 μ_B expected for a spin-only Cu(II) ion) at 2.0 K with the increase of the field (Fig. S6, Supporting Information).

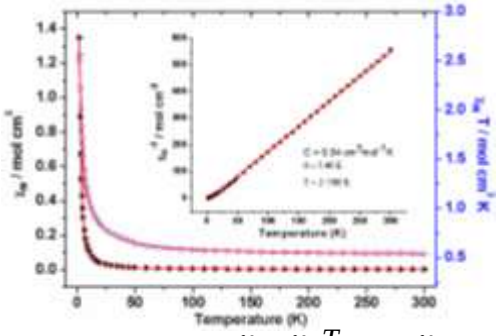

Figure 4 Temperature dependence of χ_M , $\chi_M T$, and 1/ χ_M collected in an applied field of 1000 K for complex **3**. The red solid line represents the best fittings.

The thermal variation at the range of 2.0−300 K follows the Curie-Weiss law with C = 0.54 cm^3 K mol^{-1} and θ = 5.40 K. To further evaluate the interaction (J) between Cu(II) ions, we employed a Heisenberg ferromagnetic S = 1/2 chain based on the Hamiltonian $\hat{H} = -J\sum \hat{S}_i \hat{S}_{i+1}$ to consider the intra-chain magnetic exchange interaction. where J is the exchange interaction parameter of adjacent Cu(II) ions. Thus, the magnetic data of **3** is fitted by Eqn. (4):

$$\chi_{chain} = \frac{N_A g^2 \mu_B{}^2}{4kT}\left(\frac{A}{B}\right)^{\frac{2}{3}} \qquad (4)$$

Wherein A = 1.0 + 5.7979916x + 16.902653x^2 + 29.376885x^3 + 29.832959x^4 + 14.036918x^5, B =1.0 + 2.7979916x + 7.0086780x^2 + 8.6538644x^3 + 4.5743114x^4, and $x = J/2kT$.

$$\chi_M = \frac{\chi_{chain}}{1 - \frac{2zj' \times \chi_{chain}}{N_A g^2 \mu_B{}^2}} \qquad (5)$$

The best fit for **3** in the temperature range of 2.0−300 K gives g = 2.34(1), J = 9.28(1) cm^{-1}, and zj' = −0.068(3) cm^{-1} with an agreement factor of $R = \sum(\chi_M T_{exp} - x_M T_{cal})^2 / \sum(\chi_M T_{exp})^2$ is 1.8 × 10^{-4}. The facts of θ > 0 and J > 0 indicate that there is ferromagnetic interactions between neighboring Cu(II) ions for the complex **3**. The intrachain ferromagnetic coupling in complex **3** is in agreement with the well-known ability of the *syn-anti* carboxylate bridge to mediate weak ferro- or antiferromagnetic interactions,[31] features which have been substantiated by density functional theory (DFT) type calculations for dinuclear Cu(II) complexes.[32] Actually, being similar to [Fe(pyoa)$_2$]$_n$ (pyoa = 2-(pyridin-3-yloxy)acetate)[14], a remarkable Jahn-Teller distortion exists in the complex **3**. The

unpaired electron of the Cu(II) ion is essentially described by a magnetic orbital built from the $d_{x^2-y^2}$ metallic orbital and located mainly in the basal plane with some possible admixture of a z^2 type orbital. From the structural analysis, the *syn-anti* coordination modes induce ferromagnetic exchange of the order of a few complexes in the basal-basal configuration and antiferromagnetic interactions in the range of few complexes in the axial-basal configuration.[33] In addition, For the nonplanar Cu−O−C−O'−Cu' skeleton with a *syn-anti* basal (1.971(1) Å)−basal (1.981(4) Å) bridging mode, might cause a reduction of the antiferromagnetic contribution to such an extent that the ferromagnetic contribution becomes predominant.[28a]

Magnetic properties of the isostructures with 3d-electron-rich metal ions.

In general, the ordered magnetic structure of a magnetic complex is determined by spin exchange interactions, and the electronic effects due to the different carboxylate bridge.[5a]

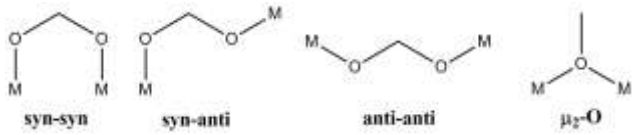

Scheme 3 The main bridging modes of the carboxylate ligand.

Magnetic studies on the 3d-electron-rich metal complexes with linear chains in the series have indicated spin coupling through carboxylate bridges,[7c, 34] and the spin exchanges of $M_2(CO_2)_n$ (M = Mn, Fe, Co, Ni, Cu) occur through the M−O−C−O−M or M−O−M exchange paths between adjacent M(II) ion sites.[14, 35] Among the exchange pathway between the nearest neighboring metal ions, anti- or ferromagnetic couplings occur depending on the carboxylate bridging modes (Scheme 3) and the geometry characters of the metal ions.

In the common view, the bridging carboxylic groups with *anti−anti* mode mediate the antiferromagnetic coupling between adjacent spin carriers due to the geometry of the magnetic orbital.[5a] Moreover, the exchange interaction between two M(II) ions bridged by the double *syn−syn* carboxyl bridges is also dominantly antiferromagnetic, and that bridged through the *syn−anti* carboxyl bridges is weak ferro- or antiferromagnetic.[8a, 36] Whereas there are a lot of copper(II) complexes with *syn−anti* configuration, , but iron(II) and nickel(II) complexes with *syn−anti* configuration of sole M−O−C−O−M bridge model are scarce. As we expect that, compared with the reported complexes,[37] quite similar interactions develop within the ribbon chain of the new 3D complexes.

The complexes of the ligand H_2bpta^{2-} bonded to 3d-electron-rich metal ions (abbreviated $[Mn(H_2bpta)]_n$,[20] $[Fe(H_2bpta)]_n$, $[Co(H_2bpta)]_n$,[20] $[Ni(H_2bpta)]_n$, $[Cu(H_2bpta)]_n$) have isostructural and sole *syn−syn* carboxyl bridging features. Magnetic data are compared in Table 3. As a result, the magnetic members of $[M_2(CO_2)_2]$ with a simple uniform chain model show different magnetic behaviors. According to previous literature, magnetic studies on the Mn(II) species in the series have most indicated antiferromagnetic coupling through sole carboxylate bridges.[7c] The $[Mn(H_2bpta)]_n$ and $[Fe(H_2bpta)]_n$ are considered as antiferrimagnet, agreeing with the above-mentioned trend. However, only a few complexes[38] exhibit weak ferromagnetic ordering above 2K related to spin canting, which have also been demonstrated in some other Mn(II) species with various bridges.

In octahedral symmetry of Co(II) complexes, high-spin S = 3/2 Co(II) ions have an orbitally degenerate $^4T_{1g}$ ground electronic term. Since the unquenched orbital momentum and the consequent spin−orbital coupling intrinsic to octahedral Co(II) impart strong magnetic anisotropy to the chain in Co(II) complexes, the isotropic classical spin model used for complex **1** is not valid for $[Co(H_2bpta)]_n$ complex. Hence, the ultimate ferromagnetic coupling between Co(II) ions, fitted by an expression[20] for S = 3/2 systems with dominant zero-field splitting effects (D), dominates the magnetic properties of Co(II) complex. Nevertheless, magneto-structural studies on

Table 3 Magnetic Parameters Associated with the M−O···O−M Spin Exchange Paths in [M(H2bpta)]n (M = Mn(II), Fe(II), Co(II), Ni(II), Cu(II))

	Mn(II)	Fe(II)	Co(II)	Ni(II)	Cu(II)	Zn(II)
$3d^n$	d^5	d^6	d^7	d^8	d^9	d^{10}
S	5/2	2	3/2	1	1/2	0
Ground state	$^6A_{1g}$	$^5T_{2g}$	$^4T_{1g}$	$^3A_{2g}$	^2E_g	$^1A_{1g}$
C	4.29	4.09	4.34	1.43	0.54	—
θ (K)	—	−7.59	−42.2	3.20	5.40	—
g	2.21	2.25	2.69	2.38	2.34	—
J (cm^{-1})	−0.12	−0.81	0.92	3.67	9.28	—
zj' (cm^{-1})	−0.92	−0.036	—	−0.070	−0.068	—
Magnetism[1]	AF	AF	F	F	F	D
Ref	20	This work	20	This work	This work	

[1]AF for anti-ferromagnetism, F for ferromagnetism, and D for diamagnetism.

hexa-coordinated Fe(II)/Ni(II) complexes with the *syn-anti* carboxylate bridge are scarce. Ferromagnetic interactions are known to be dominant in Ni(II) and Cu(II) complexes with very few exceptions. In turn, antiferromagnetic interactions have been described for Mn(II) and Co(II) system.

Generally speaking, carboxylate bridges can efficiently mediate either ferromagnetic (FM) or antiferromagnetic (AFM) coupling, depending mainly upon the bridging mode and the metal ion.Visibly, the magnetic properties of the complex **1** are different from those of the complexes **2** and **3**, although they are isostructural in crystal structures. To our knowledge, the magnetic properties of a complex mostly come from the electronic species of metal and non-metal as well as

their bond modes. In our examples, the complexes have the same *syn-anti* bridging modes with the different M−O bond bond lengths (see Table 2) and M…M distances in **1-3** (4.880(2), 4.784(2) and 4.541(2) Å, respectively) and different metal ions (Fe(II), Ni(II) and Co(II)), which are not isoelectronic species. Further evaluation of this difference might come from the method of neutron diffraction.

More studies[5c, 7b, 8d, 39] concerned with different double bridges chain metal complexes. These correlations indicate that M–O–M border line angle of about 100° for the magnetism is significant. The difference in the magnitude and the sign of the magnetic exchange interactions found for these complexes[5a] can be satisfactorily explained in terms of the kind of bridged ligands and the interaction between the metal centers and ligands.

Conclusions

In summary, we have successfully constructed four new isostructural coordination polymers from the 2,2',4,4'-biphenyltetracarboxylate ligand. Magnetic exchange interactions through carboxylate bridges between the 3d-electron-rich metal ions are ubiquitous in molecule-based magnetism, whereas complexes are scarce via sole *syn-anti* bridge model. Magnetic studies reveal the polymers with *iso*-structure features and a uniform chain model show different magnetic behaviors due to different spins. The results indicate that the presence of a weak antiferromagnetic exchange for **1** (intra-chain interaction $J = -0.81(1)$ cm^{-1}). The phenomenon of **1** is agreement with the view that the exchange interaction between two M(II) ions bridged by the *syn-anti* carboxylate bridge is dominantly weak antiferromagnetic,[8a] and the compound **2** represents a new example of the rare Fe(II) systems exhibiting the coexistence of antiferromagnetic ordering. However, magnetic studies also indicate that the presence of a weak ferromagnetic exchange for **2**−**3** (intra-chain interaction $J = 3.67(2)$ cm^{-1} for **2**, and 9.28(1) cm^{-1} for **3**, respectively.), which are in accordance with existing complexes.[5a] In addition, the M–O–C–O–M spin exchange interactions $|J|$ of $M_2(CO_2)_2$ (M = Mn(II), Fe(II), Co(II), Ni(II), Cu(II)) decrease strength in the order of $Cu_2(CO_2)_2$ > $Ni_2(CO_2)_2$ > $Co_2(CO_2)_2$ > $Fe_2(CO_2)_2$ > $Mn_2(CO_2)_2$, consistent with the orbits order. The results demonstrate that 2,2',4,4'-biphenyltetracarboxylic acid ligand can well assemble 3D CPs with intriguing architectures and different magnetic behaviors.

Acknowledgements

We gratefully acknowledge the financial support of the Natural Science Foundation of China (Grant Nos. 21171109, 21271121, and 21201113), SRFDP (Grant Nos. 20111401110002 20111401120001, and 20121401110005), the Provincial Natural Science Foundation of Shanxi Province of China (Grant Nos. 2011011009-1) and the Shanxi Scholarship Council of China (2012-004) for financial support.

References

1 (*a*) M. O'Keeffe and O. M. Yaghi, *Chem. Rev.*, 2012, **112**, 675-702; (*b*) M. Li, D. Li, M. O'Keeffe and O. M. Yaghi, *Chem. Rev.*, 2014, **114**, 1343-1370; (*c*) R. D. Kennedy, D. J. Clingerman, W. Morris, C. E. Wilmer, A. A. Sarjeant, C. L. Stern, M. O'Keeffe, R. Q. Snurr, J. T. Hupp, O. K. Farha and C. A. Mirkin, *Cryst. Growth Des.*, 2014, **14**, 1324-1330.

2 (*a*) J. P. Zhang, Y. B. Zhang, J. B. Lin and X. M. Chen, *Chem. Rev.*, 2012, **112**, 1001-1033; (*b*) Q. Yang, D. Liu, C. Zhong and J. R. Li, *Chem. Rev.*, 2013, **113**, 8261-8323; (*c*) M. P. Suh, H. J. Park, T. K. Prasad and D. W. Lim, *Chem. Rev.*, 2012, **112**, 782-835; (*d*) A. B. Sorokin, *Chem. Rev.*, 2013, **113**, 8152-819; (*e*) W. Zhang and R. G. Xiong, *Chem. Rev.*, 2012, **112**, 1163-1195; (*f*) C. Wang, T. Zhang and W. Lin, *Chem. Rev.*, 2012, **112**, 1084-1104; (*g*) P. Horcajada, R. Gref, T. Baati, P. K. Allan, G. Maurin, P. Couvreur, G. Ferey, R. E. Morris and C. Serre, *Chem. Rev.*, 2012, **112**, 1232-1268; (*h*) H. Sato, W. Kosaka, R. Matsuda, A. Hori, Y. Hijikata, R. V. Belosludov, S. Sakaki, M. Takata and S. Kitagawa, *Science*, 2014, **343**, 167-170; (*i*) G. Barin, V. Krungleviciute, D. A. Gomez-Gualdron, A. A. Sarjeant, R. Q. Snurr, J. T. Hupp, T. Yildirim and O. K. Farha, *Chem. Mat.*, 2014, **26**, 1912-1917.

3 (*a*) S. T. Zheng, T. Wu, C. Chou, A. Fuhr, P. Feng and X. Bu, *J. Am. Chem. Soc.*, 2012, **134**, 4517-4520; (*b*) B. Zheng, J. Bai, J. Duan, L. Wojtas and M. J. Zaworotko, *J. Am. Chem. Soc*., 2011, **133**, 748-751; (*c*) J. A. Botas, G. Calleja, M. Sanchez-Sanchez and M. G. Orcajo, *Langmuir*, 2010, **26**, 5300-5303; (*d*) J. M. Taylor, R. Vaidhyanathan, S. S. Iremonger and G. K. Shimizu, *J. Am. Chem. Soc.*, 2012, **134**, 14338-14340.

4 (*a*) Y. Zhou, M. Hong and X. Wu, *Chem. Commun.*, 2006, 135-143; (*b*) J. M. Zhou, W. Shi, N. Xu and P. Cheng, *Cryst. Growth Des.*, 2013, **13**, 1218-1225; (*c*) X. Q. Lü, J. J. Jiang, C. L. Chen, B. S. Kang and C. Y. Su, *Inorg. Chem.*, 2005, **44**, 4515-4521; (*d*) T. F. Liu, J. Lu and R. Cao, *CrystEngComm*,, 2010, **12**, 660-670; (*e*) Q. Sun, A. L. Cheng, Y. Q. Wang, Y. Ma and E. Q. Gao, *Inorg. Chem.*, 2011, **50**, 8144-8152; (*f*) C. Maxim, D. G. Branzea, C. Tiseanu, M. Rouzieres, R. Clerac, M. Andruh and N. Avarvari, *Inorg. Chem.*, 2014, **53**, 2708-2717; (*g*) J. M. Cameron, G. N. Newton, C. Busche, D. L. Long, H. Oshio and L. Cronin, *Chem. Commun.*, 2013, **49**, 3395-3397.

5 (*a*) X. Y. Wang, H. Y. Wei, Z. M. Wang, Z. D. Chen and S. Gao, *Inorg. Chem.*, 2005, **44**, 572-583; (*b*) Z. M. W. Z. He, S. Gao and C. H. Yan, *Inorg. Chem.*, 2006, **45**, 6694-6705; (*c*) C. J. Milios, A. Prescimone, J. Sanchez-Benitez, S. Parsons, M. Murrie and E. K. Brechin, *Inorg. Chem.*, 2006, **45**, 7053-7055.

6 (*a*) F. Su, L. P. Lu, S. S. Feng and M. L. Zhu, *CrystEngComm*, 2014, 16, 7990-7999; (*b*) E. Coronado, J. R. Galan-Mascaros, C. J. Gomez-Garcia and A. Murcia-Martinez, *Chem. Eur. J.*, 2006, **12**, 3484-3492; (*c*) E. Colacio, J. M. DomÍnguez-Vera, M. Ghazi, R. Kivekäs, M. Klinga and J. M. Moreno, *Eur. J. Inorg. Chem.* **1999**, 441-445; (*d*) J. Y. Zhang, K. Wang, X. B. Li and E. Q. Gao, *Inorg. Chem.*, 2014, **53**, 9306-9314.

7 (*a*) Y. W. Ren, J. X. Lu, B. W. Cai, D. B. Shi, H. F. Jiang, J. Chen, D. Zheng and B. Liu, *Dalton Trans.*, 2011, **40**, 1372-1381; (*b*) H. P. Jia, W. Li, Z. F. Ju and J. Zhang, *Eur. J. Inorg. Chem.*, 2006, 4264-4270; (*c*) G. M. Zhuang, X. B. Li, Y. Q. Wen, C. Y. Tian and E. Q.

Gao, *Eur. J. Inorg. Chem.*, 2014, 3488-3498; (*d*) R. Y. Li, B. W. Wang, X. Y. Wang, X. T. Wang, Z. M. Wang and S. Gao, *Inorg. Chem.*, 2009, **48**, 7174-7180; (*e*) P. Samarasekere, X. Wang, A. J. Jacobson, J. Tapp and A. Moller, *Inorg. Chem.*, 2014, **53**, 244-256; (*f*) X. Y. Wang, Z. M. Wang and S. Gao, *Chem. Commun.*, 2008, 281-294.

8 (*a*) E. Coronado, J. R. Galan-Mascaros, C. J. Gomez-Garcia and A. Murcia-Martinez, *Chem. Eur. J.*, 2006, **12**, 3484-3492; (*b*) H. Xiang, C. Lee, H. J. Koo, X. Gong and M. H. Whangbo, *Dalton Trans.*, 2013, **42**, 823-853; (*c*) J. P. Zhao, B. W. Hu, Q. Yang, X. F. Zhang, T. L. Hu and X. H. Bu, *Dalton Trans.*, 2010, 56-58; (*d*) Z. L. Chen, C. F. Jiang, W. H. Yan, F. P. Liang and S. R. Batten, *Inorg. Chem.*, 2009, **48**, 4674-4684; (*e*) J. P. Walsh, S. Sproules, N. F. Chilton, A. L. Barra, G. A. Timco, D. Collison, E. J. McInnes and R. E. Winpenny, *Inorg. Chem.*, 2014, **53**, 8464-8472.

9 (*a*) Q. Lin, T. Wu, S. T. Zheng, X. Bu and P. Feng, *Chem. Commun.*, 2011, **47**, 11852-11854; (*b*) S. M. Cohen, *Chem. Rev.*, 2012, **112**, 970-1000; (*c*) Y. Oka, K. Inoue, H. Kumagai and M. Kurmoo, *Inorg. Chem.*, 2013, **52**, 2142-2149.

10 (*a*) G. L. Abbati, A. Cornia, A. C. Fabretti, A. Caneschi and D. Gatteschi, *Inorg. Chem.*, 1998, **37**, 3759-3766; (*b*) C. Baffert, M. N. Collomb, A. Deronzier, S. Kjaergaard-Knudsen, J. M. Latour, K. H. Lund, C. J. McKenzie, M. Mortensen, L. Nielsen and N. Thorup, *Dalton Trans.*, 2003, 1765-1772; (*c*) R. Biswas, C. Diaz, A. Bauza, M. Barcelo-Oliver, A. Frontera and A. Ghosh, *Dalton Trans.*, 2014, **43**, 6455-6467; (*d*) T. Fujihara, J. Aonahata, S. Kumakura, A. Nagasawa, K. Murakami and T. Ito, *Inorg. Chem.*, 1998, **37**, 3779-3784.

11 (*a*) J. P. Zhao, S. D. Han, R. Zhao, Q. Yang, Z. Chang and X. H. Bu, *Inorg. Chem.*, 2013, **52**, 2862-2869; (*b*) G. C. Xu, W. Zhang, X. M. Ma, Y. H. Chen, L. Zhang, H. L. Cai, Z. M. Wang, R. G. Xiong and S. Gao, *J. Am. Chem. Soc.*, 2011, **133**, 14948-14951; (*c*) L. Cañadillas-Delgado, O. Fabelo, J. Pasán, F. S. Delgado, F. Lloret, M. Julve and C. Ruiz-Pérez, *Inorg. Chem. Commun.*, 2007, **46**, 7458-7465.

12 (*a*) B. Chen, N. W. Ockwig, F. R. Fronczek, D. S. Contreras and O. M. Yaghi, *Inorg. Chem.*, 2005, **44**, 181-183; (*b*) D. Tian, Y. Pang, Y. H. Zhou, L. Guan and H. Zhang, *CrystEngComm*, 2011, **13**, 957-966; (*c*) L. X. Sun, Y. Qi, Y. M. Wang, Y. X. Che and J. M. Zheng, *CrystEngComm*, 2010, **12**, 1540-1547; (*d*) O. Fabelo, J. Pasán, L. Cañadillas-Delgado, F. S. Delgado, A. Labrador, F. Lloret, M. Julve and C. Ruiz-Pérez, *Cryst. Growth Des.*, 2008, **8**, 3984-3992; (*e*) B. Zheng, J. Luo, F. Wang, Y. Peng, G. Li, Q. Huo and Y. Liu, *Cryst. Growth Des.*, 2013, **13**, 1033-1044.

13 S. K. Dey, B. Bag, K. M. Abdul Malik, M. S. El Fallah, J. Ribas and S. Mitra, *Inorg. Chem.*, 2003, **42**, 4029-4035.

14 Y. Z. Zheng, W. Xue, M. L. Tong, X. M. Chen, F. Grandjean and G. J. Long, *Inorg. Chem.*, 2008, **47**, 4077-4087.

15 Bruker, SMART (Version 5.0) and SAINT (Version 6.02).

16 SAINTPlus, version 6.22, Bruker Analytical X-ray Systems: Madison, WI, 2001.

17 R. H. Blessing, *Acta Crystallogr.*, 1995, A**51**, 33-38.

18 Z. Otwinowski and W.Minor, *Methods Enzymol.*, 1997, **276**, 307-326.

19 G. M. Sheldrick, *Acta Crystallogr.*, 2008, **A64**, 112-122.

20 Z. R. Pan, J. Xu, X. Q. Yao, Y. Z. Li, Z. J. Guo and H. G. Zheng, *CrystEngComm*, 2011, **13**, 1617-1624.

21 (*a*) M. H. Zeng, Z. Yin, Y. X. Tan, W. X. Zhang, Y. P. He and M. Kurmoo, *J. Am. Chem. Soc.*, 2014, **136**, 4680-4688; (*b*) H. Bußkamp, G. B. Deacon, M. Hilder, P. C. Junk, U. H. Kynast, W. W. Lee and D. R. Turner, *CrystEngComm*, 2007, **9**, 394-411; (*c*) W. X. Chen, H. R. Xu, G. L. Zhuang, L. S. Long, R. B. Huang and L. S. Zheng, *Chem. Commun.*, 2011, **47**, 11933-11935.

22 J. Jia, M. Shao, T. Jia, S. Zhu, Y. Zhao, F. Xing and M. Li, *CrystEngComm*, 2010, **12**, 1548-1561.

23 (*a*) L. F. Ma, M. L. Han, J. H. Qin, L. Y. Wang and M. Du, *Inorg. Chem.*, 2012, **51**, 9431-9442; (*b*) J. M. Rueff, C. Paulsen, J. Souletie, M. Drillon and P. Rabu, *Solid State Sci.* 2005, **7**, 431-436; (*c*) J. A. McCleamey, S. Merchant and R. L.Carlin, *Inorg. Chem.* 1973, **12**, 906-908; (*d*) G. Kolks, S. J. Lippard and J. V. Waszczack, *J. Am. Chem. Soc.* 1980, **102**, 4832-4833.

24 Fisher, M. E. Am. J. Phys. 1964, **32**, 343–346.

25 A. Rodriguez-Dieguez, J. Cano, R. Kivekas, A. Debdoubi and E. Colacio, *Inorg. Chem.*, 2007, **46**, 2503-2510.

26 (*a*) T. Whitfield, L. M. Zheng, X. Wang, and A. J. Jacobson, *Solid State Sci.* 2001, **3**, 829–835; (*b*) K. O. Kongshaug, and H. Fjellvg, *Solid State Sci.* 2002, **4**, 443–447.

27 H. Oshio, N. Hoshino, T. Ito and M. Nakano, *J. Am. Chem. Soc.*, 2004, **126**, 8805-8812**.**

28 (*a*) F. T. Xie, L. M. Duan, J. Q. Xu, L. Ye, Y. B. Liu, X. X. Hu and J. F. Song, *Eur. J. Inorg. Chem.* 2004, 4375-4379; (*b*) P. S. Mukherjee, S. Konar, E. Zangrando, T. Mallah, J. Ribas and N. R. Chaudhuri. *Inorg. Chem.* 2003, **42**, 2695-2703; (*c*) M. Du, X. H. Bu, Y. M. Guo, L. Zhang, D. Z. Liao and J. Ribas. *Chem. Commun.* 2002, 1478-1479.

29 K. K. Nanda, R. Das, L. K. Thompson, K. Venkatsubramanian and K. Nag, *Inorg. Chem*. 1994, **33**, 5934-5939.

30 S. Laborda, R. Clerac, C. E. Anson and A. K. Powell, *Inorg. Chem.* 2004, **43**, 5931-5943.

31 C. Ruiz-Perez, J. Sanchiz, M. Hernandez-Molina, F. Lloret and M. Julve, *Inorg. Chem.* 2000, **39**, 1363-1370.

32 A. Rodrĺguez-Fortea, P. Alemany, S. Alvarez and E. Ruiz, *Eur. Chem.* 2001, **7**, 627-637.

33 (*a*) E. Colacio, M. Ghazi, R. Kivekäs and J. M. Moreno, *Inorg. Chem.*, 2000, **39**, 2882-2890.

34 (*a*) P. Diaz-Gallifa, O. Fabelo, J. Pasan, L. Canadillas-Delgado, J. Rodriguez-Carvajal, F. Lloret, M. Julve and C. Ruiz-Perez, *Inorg. Chem.*, 2014, **53**, 5674-5683; (*b*) X. J. Li, T. N. Guan, X. F. Guo, X. X. Li and Z. J. Yu, *Eur. J. Inorg. Chem.*, 2014, 2307-2316; (*c*) P. Seth, A. Figuerola, J. Jover, E. Ruiz and A. Ghosh, *Inorg. Chem.*, 2014, **53**, 9296-9305.

35 O. Fabelo, J. Pasán, L. Cañadillas-Delgado, F. S. Delgado, F. Lloret, M. Julve and C. Ruiz-Pérez, *Inorg. Chem.*, 2008, **47**, 8053-8061.

36 Y. Z. Zheng, W. Xue, M. L. Tong, X. M. Chen, F. Grandjean and G. J. Long, *Inorg. Chem.*, 2008, **47**, 4077-4087.

37 (*a*) W. Zhao, Y. Song, T. A. Okamura, J. Fan, W. Y. Sun and N. Ueyama, *Inorg. Chem.*, 2005, **44**, 3330-3336. (*b*) L. D. Earl, B. O. Patrick and M. O. Wolf, *Inorg. Chem.*, 2013, **52**, 10021-10030.

38 (*a*) J. L. Manson, Q. Z. Huang, J. W. Lynn, H. J. Koo, M. H. Whangbo, R. Bateman, T. Otsuka, N. Wada, D. N. Argyriou and J. S. Miller, *J. Am. Chem. Soc.*, 2000, **123**, 162-172; (*b*) M. H. Zeng,

M. C. Wu, H. Liang, Y. L. Zhou, X. M. Chen and S. W. Ng, *Inorg. Chem.*, 2007, **46**, 7241-7243; (*c*) Y. Liu, D. Liu, Y. Yu, J. Xu, X. Han and C. Wang, *CrystEngComm*, 2013, **15**, 10611-10617.

39 K. Wang, X. C. Yi, X. Wang, X. B. Li and E. Q. Gao, *Dalton Trans.*, 2013, **42**, 8748-8760.

